Assessing vesicular monoamine transport and toxicity using fluorescent false neurotransmitters

Carlie A. Hoffman[1], Meghan L. Bucher[2], Joshua M. Bradner[2], Lauren Jonas[1], Kenny Igarza[1], Gary W. Miller[1,2]*

[1]Department of Environmental Health, Rollins School of Public Health, Emory University, Atlanta, GA

[2]Department of Environmental Health Sciences, Mailman School of Public Health, Columbia University, New York, NY

Keywords: VMAT2, vesicle, monoamine, FFN, dopamine, Parkinson's disease

Abstract

Impairments in the vesicular packaging of dopamine result in an accumulation of dopamine in the cytosol. Cytosolic dopamine is vulnerable to two metabolic processes - enzymatic catabolism and enzymatic- or auto-oxidation - that form toxic metabolites and generate reactive oxygen species. Alterations in the expression or activity of the vesicular monoamine transporter 2 (VMAT2), which transports monoamines such as dopamine from the cytosol into the synaptic vesicle, result in dysregulated dopamine packaging. Here, we developed a series of assays using the fluorescent false neurotransmitter 206 (FFN206) to visualize VMAT2-mediated vesicular packaging at baseline and following pharmacological and toxicological manipulations. As proof of principle, we observed a significant reduction in vesicular FFN206 packaging after treatment with the VMAT2 inhibitors reserpine (IC_{50}: 73.09 nM), tetrabenazine (IC_{50}: 30.41 nM), methamphetamine (IC_{50}: 2.399 µM), and methylphenidate (IC_{50}: 94.33 µM). We then applied the assay to investigate the consequences on vesicular packaging by environmental toxicants including the pesticides paraquat, rotenone, and chlorpyrifos, as well as the halogenated compounds unichlor, perfluorooctanesulfonic acid, Paroil, Aroclor 1260, and hexabromocyclododecane. Several of the environmental toxicants showed minor impairment of vesicular FFN206 loading, suggesting that the toxicants are weak VMAT2 inhibitors at the concentrations tested. The assay presented here can be applied to investigate the effect of additional pharmacological compounds and environmental toxicants on vesicular function, which will provide insight into how exposures to such factors are involved in the pathogenesis of monoaminergic diseases such as Parkinson's disease, and the assay can be used to identify pharmacological agents that influence VMAT2 activity.

Introduction

Proper vesicular dopamine storage is essential for the survival of dopaminergic neurons. When dopamine is not properly packaged into the synaptic vesicle, it accumulates in the cytosol where it is susceptible to oxidation and enzymatic deamination, which when occurring in excess result in oxidative stress and subsequent cell death.[1-3] Cytosolic monoamines, including dopamine, are packaged into synaptic vesicles by the vesicular monoamine transporter 2 (VMAT2; *SLC18A2*). Given the toxic properties of cytosolic dopamine, this process is necessary to reduce potential dopaminergic toxicity.[2,4-16] In addition to sequestering monoamines, it has been shown that VMAT2 transports the neurotoxicant 1-methyl-4-phenylpyridinium (MPP^+), the toxic active metabolite of 1-methyl-4-phenyl-1,2,3,6-tetrahydropyridine (MPTP), into synaptic vesicles. MPP^+ is a potent inhibitor of complex I of the electron transport chain, and exposure to MPTP results in immediate onset of parkinsonism.[17] However, VMAT2-mediated sequestration of MPP^+ prevents its accumulation in the cytosol, thereby diminishing its neurotoxic effect and suggesting a neuroprotective role for VMAT2.[10,18-22] These data suggest a role of VMAT2 in regulating the neurotoxic effects of both endogenous (e.g. dopamine) and exogenous (e.g. MPP^+) toxicants.

While genetic deletion of VMAT2 is neonatal lethal, mice with 5% functional expression (VMAT2-LO mice), 50% functional expression (VMAT2-HET), or 200% functional expression (VMAT2-HI mice) are viable.[6,9,11,13,20,23,24] Genetic reduction of VMAT2 expression results in progressive nigrostriatal neurodegeneration as well as olfactory deficits, depressive behavior, and altered sleep latency in mice—symptoms that mimic both the motor and non-motor symptoms of Parkinson's disease (PD).[9,25-27] In addition, VMAT2-LO and VMAT2-HET mice exhibit increased cell death upon exposure to the dopaminergic neurotoxicants methamphetamine and MPTP.[4,8,9,11-13] Conversely, VMAT2-HI mice exhibit protection against the toxic consequences of

methamphetamine and MPTP.[4-6] Collectively these data suggest that while losing VMAT2 expression or activity may facilitate neuronal toxicity, an increase in expression or activity may allow VMAT2 to confer neuroprotection. For these reasons, it is essential to understand the factors that modulate VMAT2 expression and activity.

Analyses from human studies further implicate VMAT2 as a necessary mediator of neuronal health. Decreases both in the amount of, and activity of, VMAT2 have been detected in post-mortem tissue from PD patients,[28,29] and mutations in VMAT2 have been identified as causative of infantile parkinsonism.[30] Recent work has identified low-activity variants in VMAT2 that may increase the risk of PD, and gain of function polymorphisms in *SLC18A2* have been associated with decreased risk for PD.[31-33] Furthermore, data shows a decrease in VMAT2 mRNA from platelets of PD patients suggesting that a systemic deficiency in VMAT2 may be a pathologic characteristic of the disease.[34] Genetic predisposition only accounts for a portion of PD risk, the rest of which is explained by environmental exposures including manganese and the pesticides rotenone and dieldrin.[35-39] While the mechanisms by which these toxicants contribute to PD pathogenesis remain unknown, it is possible that these toxicants exert their neurotoxicity in part by affecting VMAT2 function.[40,41]

Fluorescent false neurotransmitters (FFNs) were designed as specific substrates for VMAT2 as a tool to visualize vesicular uptake. FFN206 is a fluorescent monoamine analog and substrate of VMAT2 that was first reported in 2013.[42] Here, we replicate the findings of the original study that show FFN206 can be used to investigate VMAT2-mediated vesicular uptake, and report new data at high resolution and in near real-time. Furthermore, we optimized a 96-well plate reader-based screening assay to assess VMAT2 function and the dynamics of vesicle loading under: 1) physiological conditions, 2) during treatment with pharmacological inhibitors of VMAT2, and 3)

during treatment with select pesticides and halogenated compounds. Our data show significant reductions in vesicle packaging after treatment with the VMAT2 inhibitors tetrabenazine, reserpine, methylphenidate, and methamphetamine, and modest reduction in vesicle packaging after treatment with the toxicological compounds paraquat, rotenone, unichlor, perfluorooctanesulfonic acid, Paroil, Aroclor 1260, and hexabromocyclododecane. The methods of assessing vesicle function developed here can be used to further screen pharmacological and toxicological factors that alter dopaminergic vesicular storage.

Materials and Methods

Cell culture. Human embryonic kidney cells (HEK293, ATCC) were cultured at 37°C with 5% CO_2 in media comprised of Dulbecco's Modified Eagle Medium (DMEM, Corning), 10% Fetal Bovine Serum (FBS, Atlanta Biologicals), and 1% Penicillin-Streptomycin (Pen Strep, Corning). All human VMAT2-containing constructs were made in pcDNA3.1 vectors (Life Technologies) containing a zeocin resistance gene. Plasmids were transfected into HEK293 cells with Lipofectamine 2000 using the manufacturer protocol and stable cell lines were generated by repetitive rounds of limiting dilutions in selection media. HEK293 cells stably expressing human VMAT2 (HEK+VMAT2) or mCherry-tagged human VMAT2 (HEK+mCherry-VMAT2) were cultured at 37°C with 5% CO_2 in selection media comprised of DMEM (Corning), 10% FBS (Atlanta Biologicals), 1% Pen Strep (Corning), and zeocin (100 µg/mL, InvivoGen). Experimental media used to optimize the 96-well plate screening assay and to screen pharmacological inhibitors of VMAT2 and environmental toxicants was comprised of DMEM without phenol red (Corning), 1% Pen Strep (Corning), and 1% L-glutamine (Gibco).

Live-cell total internal reflection fluorescence (TIRF) microscopy. HEK+VMAT2 cells were seeded at 60,000 cells per well on laminin-coated glass-bottom 8-well chamber dishes (LabTek) and maintained in selection media until they reached 60% confluence. Upon reaching confluence, the selection media was aspirated and replaced with experimental media containing 1 µM FFN206 (Abcam). Cells were incubated with FFN206 for 1 hour at 37°C with 5% CO_2 before the FFN206-containing media was aspirated and replaced with experimental media. Cells were then imaged at 37°C with 5% CO_2 on the GE Delta Vision OMX total internal reflection fluorescence (TIRF) microscope (FFN206 peak excitation = 369 nm; peak emission = 464 nm).

Real-time uptake with confocal microscopy. HEK+VMAT2 cells or HEK+mCherry-VMAT2 cells were seeded at 100,000 cells per plate in laminin-coated glass-bottom round 35 mm dishes (ThermoFisher) and maintained in selection media until they reached 80% confluency. Upon reaching confluency, selection media was aspirated and replaced with experimental media. Cells were imaged on a Nikon A1R TE2000 confocal microscope at 37°C with 5% CO_2. Cells were imaged for a 30 second baseline before the addition of FFN206 to a final concentration of 20 µM. Imaging lasted for a duration of 5 minutes or 1000 seconds (16.67 minutes; FFN206 peak excitation = 369 nm; peak emission = 464 nm; mCherry peak excitation = 587 nm; peak emission = 610 nm).

96-well plate screening assay. We adapted the protocol utilized by Hu and colleagues[42] for use in a 96-well plate reader. HEK+VMAT2 cells were seeded at 40,000 cells per well in half volume, black-walled, laminin-coated 96-well plates (Grenier Bio One) and maintained in selection media at 37^{o}C with 5% CO_2 until 90-100% confluent (approximately 24 hours). Upon reaching

confluency, selection media was aspirated and replaced with 90 µL of either experimental media or experimental media containing the desired pharmacological compound or environmental toxicant. Plates were incubated with the pharmacological compound and/or environmental toxicant for 30 minutes at 37°C with 5% CO_2 before FFN206 (Abcam) was diluted in experimental media and added to the appropriate wells to produce a final concentration of 1 µM FFN206 per well. Plates were incubated with FFN206 for 60 minutes at 37°C with 5% CO_2. Wells were then washed with sterile phosphate-buffered saline (PBS, Gibco) and imaged in PBS on a BioTek Synergy H1 multi-mode plate reader (FFN206 peak excitation = 369 nm; peak emission = 464 nm).

Concentrations of pharmacological compounds and environmental toxicants. Tetrabenazine (Sigma) was diluted in experimental media to a final concentration of 10 µM per well/plate for the negative control group and to concentrations of 0.0001, 0.001, 0.01, 0.1, 1, and 10 µM to produce a dose response curve. Bafilomycin (InvivoGen) was diluted in experimental media to a final concentration of 1 µM per well/plate. Reserpine was diluted in experimental media to final concentrations of 0.0001, 0.001, 0.01, 0.1, 1, and 10 µM. Methamphetamine and methylphenidate were diluted in experimental media to final concentrations of 0.01, 0.1, 1, 10, and 100 µM. Stock concentrations of rotenone, paraquat, chlorpyrifos, unichlor, PFOS, Paroil, hexabromocyclododecane, and Aroclor 1260 were dissolved in dimethyl sulfoxide (DMSO, Fisher) and then diluted in experimental media into a 200 µM working stock. From this working stock, each compound was diluted in experimental media to final concentrations of 0.01, 0.1, 1, 10 and 100 µM.

Statistical analysis. The data were analyzed by t-test, ANOVA, and z factor analysis as appropriate using GraphPad Prism software. The z factor is commonly used in the design of protocols for high-throughput screens and incorporates the positive control mean (μ_+), the positive control standard deviation (σ_+), the negative control mean (μ_-), and the negative control standard deviation (σ_-) [42].

$$Z = 1 - \frac{(3\sigma_+ + 3\sigma_-)}{|\mu_+ - \mu_-|}$$

Results

FFN206 packaging is dependent on VMAT2 function. We first sought to confirm that FFN206 fluorescence was a reliable representation of VMAT2-mediated vesicular uptake. To this end, HEK cells stably transfected with mCherry-tagged human VMAT2 (HEK+mCherry-VMAT2) were treated with 1 µM FFN206, and FFN206 fluorescence was recorded after one hour of incubation. FFN206 fluorescence was observed to overlap with VMAT2 fluorescence (Figure 1A), thus confirming that FFN206 was loaded into VMAT2-containing cells. Furthermore, analysis of HEK+VMAT2 cells grown in a glass-bottom 8-chamber dish following incubation with 1 µM FFN206 using a GE Delta Vision OMX Blaze TIRF microscope demonstrated the localization of FFN206 fluorescence within small vesicle-like compartments at high resolution (60x magnification) within live cells (Figure 1B).

To further confirm that FFN206 was loaded via VMAT2 into vesicular compartments, HEK cells stably transfected with human VMAT2 (HEK+VMAT2) were treated with 10 µM tetrabenazine (TBZ) – a pharmacological inhibitor of VMAT2. Compared to HEK cells lacking VMAT2 that show no FFN206 uptake, treatment with tetrabenazine resulted in almost total loss of FFN206 fluorescence in HEK + VMAT2 cells, indicating that VMAT2 function must be

maintained in order to observe FFN206 fluorescence (Figure 1C). Quantification of FFN206 fluorescence displayed as percent control demonstrated a significant increase in fluorescence in HEK+VMAT2 cells treated with FFN206 than all other conditions (Figure 1D). As an additional method of confirmation, cells were treated with bafilomycin, which inhibits the vesicular ATPase that maintains the proton gradient present across the vesicular membrane that VMAT2 depends on for sequestering dopamine. As expected, bafilomycin also depleted FFN206 fluorescence (data not shown).

Real-time VMAT2-mediated uptake of FFN206. After examining FFN206 packaging in high-resolution in a live cell, we sought to observe the dynamic packaging of FFN206 in living cells in real-time. To that end, HEK+mCherry-VMAT2 cells were grown in glass-bottom round dishes and recorded a baseline of mCherry and background fluorescence for 30 seconds. Cells were then treated with 20 µM FFN206 and fluorescence was recorded for 5 minutes. Image stills from 0.93s, 3.18s, 3.94s, and 5.94s demonstrate that over time, FFN206 fluorescence and its co-localization with the VMAT2-containing vesicles is observed (Figure 2A). We then sought to examine how perturbations in VMAT2 function and vesicle function affected uptake and retention of FFN206. Uptake was recorded under four conditions: HEK cells without VMAT2 (HEK), HEK cells with human VMAT2 (HEK+VMAT2), HEK+VMAT2 cells with VMAT2 inhibitor tetrabenazine (HEK+VMAT2+TBZ), and HEK+VMAT2 cells with the proton gradient dissipater bafilomycin (HEK+VMAT2+BAF). FFN206 fluorescence was recorded for 1000 seconds in each condition (16.67 minutes), and quantification was performed on the fluorescence in the final 20 seconds of the 1000 second uptake time-course. HEK+VMAT2 cells displayed significantly greater fluorescence than HEK cells and HEK+VMAT2 cells treated with tetrabenazine or bafilomycin

193 (Figure 2B) (One-way ANOVA with Dunnett's multiple comparisons post-hoc test **** p
194 <0.0001 vs. control column HEK+VMAT2).
195
196 *Optimizing parameters for a 96-well plate assay.* We adapted the protocol utilized by Hu and
197 colleagues (2013) for use in our 96-well plate assay. In developing this protocol, we first
198 determined which concentration of FFN206 would produce a dynamic range of fluorescence in the
199 HEK+VMAT2 cell line. To this end, HEK+VMAT2 cells were treated with FFN206 at 0.0001,
200 0.001, 0.01, 0.1, 1, and 10 µM concentrations. There was a positive relationship between
201 fluorescence and FFN206 concentration; however, variability in FFN206 fluorescence scaled with
202 the increase in signal strength (Figure 3A, C). Furthermore, the fluorescence emitted by 10 µM
203 FFN206 approached the peak signal that can be detected by the 96-well plate reader, thus making
204 detection of subtle alterations in FFN206 fluorescence at this concentration unrealistic. Therefore,
205 a mid-level dose of 1 µM FFN206 was chosen for use in further experiments to ensure the assay
206 had the dynamic range necessary to detect both potential decreases and increases in VMAT2
207 function.
208 The Hu (2013) protocol utilized tetrabenazine as a negative control; thus, we performed a dose
209 response of tetrabenazine-suppressed FFN206 fluorescence to determine the appropriate
210 tetrabenazine dose to utilize in our cell line. HEK+VMAT2 cells were treated with tetrabenazine
211 at 0, 0.0001, 0.001, 0.01, 0.1, 1, and 10 µM concentrations (Figure 3B, D). The dose of
212 tetrabenazine was selected in order to achieve a good dynamic range with a high degree of FFN206
213 fluorescence suppression with the selected tetrabenazine concentration. With increasing
214 tetrabenazine concentration, FFN206 fluorescence decreased with the greatest suppression of
215 FFN206 fluorescence at 10 µM tetrabenazine; thus, this dose was chosen for the assay.

High-throughput assays require a high degree of accuracy and sensitivity, and therefore demand a wide dynamic range and minimal variability within the datasets. The z factor is commonly used in the design of protocols for high-throughput screens and incorporates the positive control mean (μ_+), the positive control standard deviation (σ_+), the negative control mean (μ_-), and the negative control standard deviation (σ_-).[43] Z factor calculation ensures that assays with favorable z values (as close to 1 as possible) will have a large band of separation between the distributions of the data for the positive and negative control. A z factor above 0.5 represents a suitable assay. For the FFN206 assay, the positive control was represented by HEK+VMAT2 cells treated with 1 µM FFN206 and 0 µM tetrabenazine, while the negative control was represented by HEK+VMAT2 cells treated with 1 µM FFN206 and 10 µM tetrabenazine. After performing iterative experiments to optimize cell density, incubation time, and reaction volume, a z factor of 0.76 was consistently achieved, indicating that the protocol was suitable for high-throughput screening (Figure 3E).

Pharmacological inhibitors of VMAT2. After optimizing the 96-well plate protocol, the assay was used to test a variety of pharmacological VMAT2 inhibitors to demonstrate the utility and accuracy of the assay. Dose-dependent VMAT2 inhibition was observed in HEK+VMAT2 cells treated with reserpine, tetrabenazine, methamphetamine, and methylphenidate from a range of 0.0001 to 10 µM to determine the concentration at which VMAT2 was completely inhibited (Figure 4). HEK+VMAT2 cells treated tetrabenazine yielded an IC_{50} of 73.09 nM and showed essentially complete inhibition at 1 µM. HEK+VMAT2 cells treated with reserpine yielded an IC_{50} of 30.41 nM and showed essentially complete inhibition at 0.1 µM. HEK+VMAT2 cells treated with methamphetamine yielded an IC_{50} of 2.399 µM and showed total inhibition by 100 µM. HEK+VMAT2 cells treated with methylphenidate yielded an IC_{50} of 94.33 µM.

Environmental toxicants and VMAT2 function. The optimized assay was then used to test a variety of pesticides (Figure 5A) and halogenated environmental toxicants (Figure 5B) of interest. All compounds were tested at concentrations of 0.01, 0.1, 1, 10 and 100 µM. The pesticides rotenone and chlorpyrifos caused a minor decrease in FFN206 uptake at the highest concentration, however, paraquat demonstrated a more significant effect on FFN206 fluorescence yielding an IC_{50} of 12.41 µM (Figure 5A). The halogenated compounds unichlor, PFOS, and hexabromocyclododecane did not show impairment of vesicular loading at the concentrations tested (Figure 5B). However, Paroil and Arochlor 1260 showed modest effects on FFN206 fluorescence with IC_{50}s of 57.03 µM and 95.07 µM respectively (Figure 5B).

Discussion

Here, we demonstrate the utility of using false fluorescent neurotransmitters to investigate the effect of pharmacological and environmental compounds on vesicular uptake in an *in vitro* application. Importantly, we were able to reproduce key findings from Hu *et al.* 2013 demonstrating that FFN206 can be used to examine VMAT2 function and the dynamics of vesicle packaging in HEK293 cells. We further went on to optimize a fluorescent 96-well plate assay with a dynamic range that allows for detection of altered VMAT2-mediated vesicular uptake and is amenable to high-throughput screening. We previously developed an assay (Bernstein *et al.* 2012) to spatially resolve VMAT2-mediated packaging of dopamine utilizing high-content imaging with a fluorescent dye and mCherry-tagged VMAT2, but this assay required time-intensive image analysis to obtain suitable results.[44] The advent of FFN206 allowed us to adapt our assay to a fluorescent plate reader format and to visualize monoamine transport with an ease and in a real-

time manner that was previously inaccessible. The methods presented here can be used in experimental applications to understand how pharmacological and environmental manipulation affects vesicle function and thus may contribute to monoaminergic neuron vulnerability.

FFN206 as a tool to visualize VMAT2-dependent vesicular uptake

Fluorescent false neurotransmitters were developed as specific substrates of VMAT2 for the purpose of visualizing monoamine uptake and release.[42,45-49] Previous work characterized vesicular uptake of FFN206 in HEK cells stably transfected with rat VMAT2,[42] and we first sought to replicate these findings in HEK cells stably transfected to express human VMAT2. We demonstrated that FFN206 fluorescence overlapped with mCherry-tagged human VMAT2 fluorescence, indicating that FFN206 is loaded into VMAT2-containing cells. Furthermore, treatment with tetrabenazine resulted in almost total loss of FFN206 fluorescence, indicating that VMAT2 function must be maintained in order to observe FFN206 fluorescence. As an additional piece of evidence, TIRF-level resolution of FFN206 packaging revealed the localization of FFN206 fluorescence to small vesicle-like compartments present in a single HEK+VMAT2 cell.

Real-time visualization of FFN206 vesicular uptake

We next sought to determine whether FFN206 could be used to measure real-time VMAT2-mediated monoamine uptake. FFN206 uptake was recorded under four conditions: HEK cells not expressing VMAT2, HEK cells expressing human VMAT2, HEK+VMAT2 cells incubated with tetrabenazine, and HEK+VMAT2 cells incubated with bafilomycin. Quantification of FFN206 fluorescence demonstrated significant differences in HEK cells lacking VMAT2 and HEK cells treated with tetrabenazine and bafilomycin compared to HEK cells expressing human VMAT2.

These results were as expected as tetrabenazine inhibits VMAT2 activity, thus preventing the sequestration of FFN206. While cells treated with bafilomycin also exhibit decreased FFN206 fluorescence, this is caused by a different mechanism. Bafilomycin inhibits the vacuolar H^+ ATPase present on vesicles, leading to the dissipation of the vesicular proton gradient present across the vesicular membrane. As the proton gradient dissipates, the physiological state of the vesicle is disrupted, and vesicular homeostasis cannot be maintained despite the continued normal function of VMAT2. Thus, the decrease in FFN206 fluorescence of HEK+VMAT2 cells treated with bafilomycin represent the necessity of proton motive force to sequester FFN206 within vesicles.

Pharmacological and toxicological applications of high-throughput FFN206 assay

We adapted the protocol utilized by Hu *et al.* for use in our 96-well plate assay for high-throughput screening applications.[42] We chose concentrations of 1 µM FFN206 and 10 µM tetrabenazine to ensure the assay had the dynamic range necessary to detect both decreases and increases in VMAT2 function. These concentrations were determined by our own dose-response experiments and reproduce the optimal concentrations determined by Hu *et al.* 2013. Iterative experiments were conducted to refine the protocol until a z score above 0.70 was consistently achieved. We further verified the reliability of the assay by screening pharmacological compounds known to inhibit VMAT2: tetrabenazine, methamphetamine, methylphenidate, and reserpine, and observed dose-dependent VMAT2 inhibition that aligned with previously published results.[42]

After confirming the reliability of the FFN206 assay, we treated HEK+VMAT2 cells with select pesticides and halogenated environmental toxicants. There is an association between exposure to environmental toxicants and PD and it has long been established that exposure to heavy metals

and pesticides contribute to PD risk.[36-39,50-54] The extent to which altered VMAT2 function mediates the toxicity of exposure to these environmental toxicants has not been extensively studied. Thus, we tested representative pesticides and halogenated environmental toxicants including rotenone, paraquat, chlorpyrifos, unichlor, PFOS, Paroil, HBCD, and Aroclor 1260 for their effect on VMAT2 function. Of these compounds, exposures to rotenone and paraquat have been most extensively associated with PD in both humans and animal models.[52,53,55]

Rotenone is a known inhibitor of mitochondrial complex I and exerts its toxicity by oxidizing mitochondrial proteins and causing oxidative stress that leads to cell death.[56,57] Similarly, paraquat exerts its toxicity predominantly through oxidative modification of cytosolic proteins, which causes oxidative stress and leads to cell death.[55,57,58] Here, we detected a reduction in VMAT2 function with administration of 100 µM of rotenone and with 10 µM and 100 µM of paraquat, though this reduced VMAT2 activity occurred at such high doses as to be physiologically irrelevant. Previous studies examining rotenone and paraquat toxicity have observed 70-80% cell death resulting from mitochondrial complex I inhibition with doses of 100 nM rotenone and 200 µM paraquat.[52,57,58] The present study differs from these studies in several respects, the first of which being the length of exposure. We exposed cells to each toxicant for a total of 90 minutes (30-minute incubation with the toxicant followed by a 60-minute incubation with FFN206), while previous studies examined toxicity after 48 hours. We also screened for VMAT2 function and not cell death. As the amount of cell death imposed by a 90-minute length of exposure is minimal, we did not assess cell death in our assay. Finally, given the high IC_{50} value we determined for paraquat and rotenone exposure, the mild inhibition of VMAT2 caused by exposures to these toxicants is not likely to be mediated by mitochondrial complex I inhibition.

For the halogenated compounds, we observed a mild reduction in VMAT2 function at high concentrations. While previous literature indicates exposure to PFOS[59], Aroclor 1260[7], and hexabromocyclododecane[60] exerts toxicity on the dopamine system, our results indicate that unichlor, PFOS, Paroil, Aroclor 1260, and hexabromocyclododecane are weak inhibitors of VMAT2 over the course of a short-term exposure, and therefore it is unlikely that these compounds affect VMAT2 function at environmentally and physiologically relevant concentrations.

Conclusions

In conclusion, we have used FFN206 to investigate VMAT2-mediated vesicle uptake at high resolution and in near real-time. Importantly, we were able to reproduce in HEK cells expressing human VMAT2 the findings reported by Hu *et al.* 2013 performed in HEK cells expressing rat VMAT2. We further optimized a 96-well plate assay that has a dynamic range and is amenable to a high-throughput format, and we used this assay to assess VMAT2 function and the dynamics of vesicle loading upon exposure to pharmacological and environmental compounds. We observed a robust reduction in VMAT2 function after exposure to tetrabenazine, reserpine, methamphetamine, and methylphenidate, and observed a modest reduction in VMAT2 function after short-term exposure to high concentrations of environmental toxicants, though inhibition of VMAT2 is unlikely to contribute to the mechanism of action of these compounds at physiologically and environmentally relevant concentrations. The methods of assessing vesicle function discussed here can be used to assess how other pharmacological and environmental compounds exert their toxicity at the level of the vesicle. These assays can provide evidence of potential mechanism by which exposures contribute to the progression of monoaminergic diseases such as Parkinson's disease.

Corresponding Author

Gary W. Miller, gary.miller@columbia.edu

Environmental Health Sciences, Mailman School of Public Health, Columbia University.

722 168th Street, New York, NY 10032

Author Contributions

The manuscript was written through contributions of all authors. All authors have given approval to the final version of the manuscript.

Funding Sources

This work was supported by NIEHS R01ES023839, NIEHS P30ES019776, and the Lewis Dickey Memorial Fund to G.W.M.; and T32ES012870 to C.A.H.

ACKNOWLEDGMENT

We would like to acknowledge Bethany Wilson for her assistance in the initial stages of method development for the 96-well plate assay. This research project was also supported in part by the Emory University Integrated Cellular Imaging Microscopy Core.

ABBREVIATIONS

VMAT2, vesicular monoamine transporter 2; FFN, fluorescent false neurotransmitter; MPTP, 1-methyl-4-phenyl-1,2,3,6-tetrahydropyridine; MPP^+, 1-methyl-4-phenylpyridinium; PD, Parkinson's disease; HEK, human embryonic kidney; PFOS, perfluorooctanesulfonic acid.

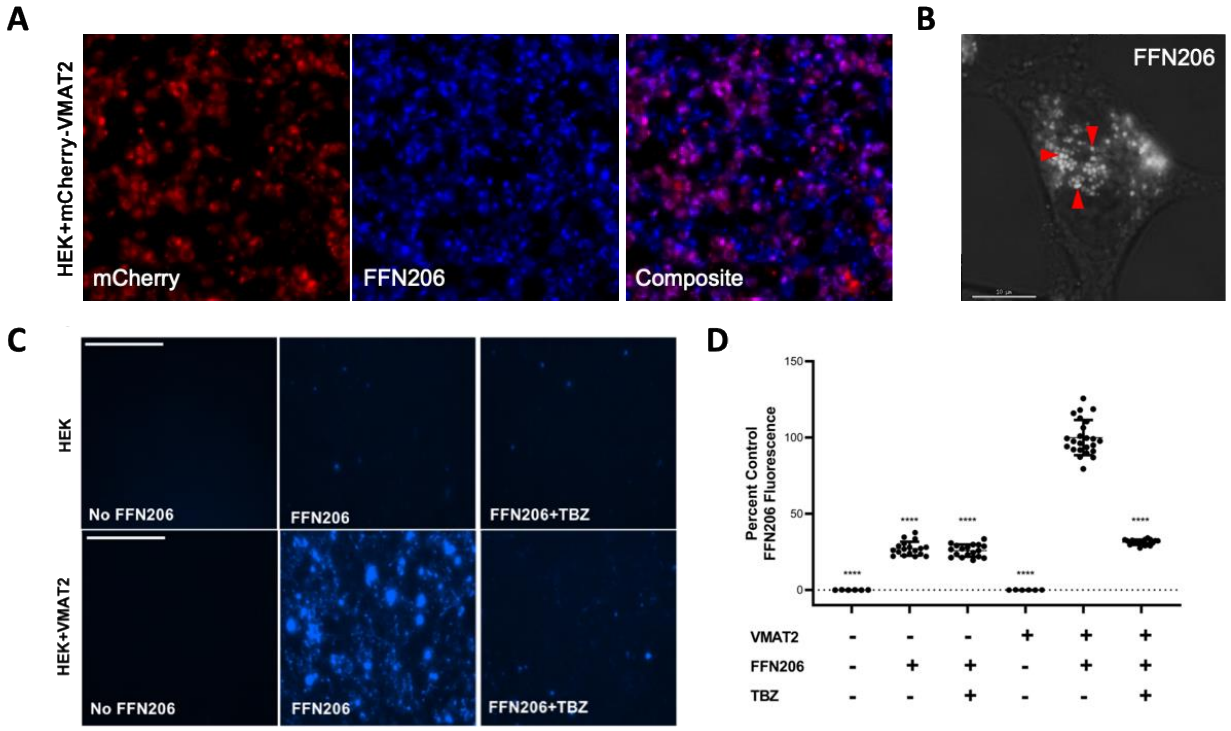

Figure 1. FFN206 packaging is dependent on VMAT2 function and maintenance of the vesicular proton gradient.

A. Representative 10x image of HEK cells stably transfected with mCherry-tagged VMAT2 (HEK+mCherry-VMAT2, left image) treated with FFN206 (center image). FFN206 fluorescence overlaps with VMAT2 fluorescence (purple, right image). B. Representative 60x TIRF microscope image demonstrates FFN206 fluorescence localized within vesicle-like compartments in a stably transfected HEK cell with VMAT2 (HEK+VMAT2), as denoted by red arrows. Scale bar = 10 µM. C. Representative images of FFN206 fluorescence in control HEK cells with and without VMAT2. In control HEK cells (top), there was no background fluorescence in the absence of FFN206 (left). FFN206 treatment exhibited minimal fluorescence (middle), and FFN206 fluorescence was unchanged following treatment with the VMAT2 inhibitor tetrabenazine (10 µM) (right). Representative images of FFN206 fluorescence in HEK+VMAT2 cells (bottom). In the absence of FFN206, no background fluorescence is observed in HEK+VMAT2 cells (left).

HEK+VMAT2 cells treated with FFN206 exhibit robust fluorescence (middle) that was diminished when VMAT2 function is inhibited by treatment with 10 μM tetrabenazine (right). D. Quantification of FFN206 fluorescence from panel C. Data displayed as percent control mean and standard error of the mean, with the control group being HEK+VMAT2 cells incubated with FFN206. Each point represents one well of cells from a 96-well plate. (One-way ANOVA with Dunnett's multiple comparisons post-hoc test **** $p < 0.0001$ vs. control column HEK+VMAT2+FFN206).

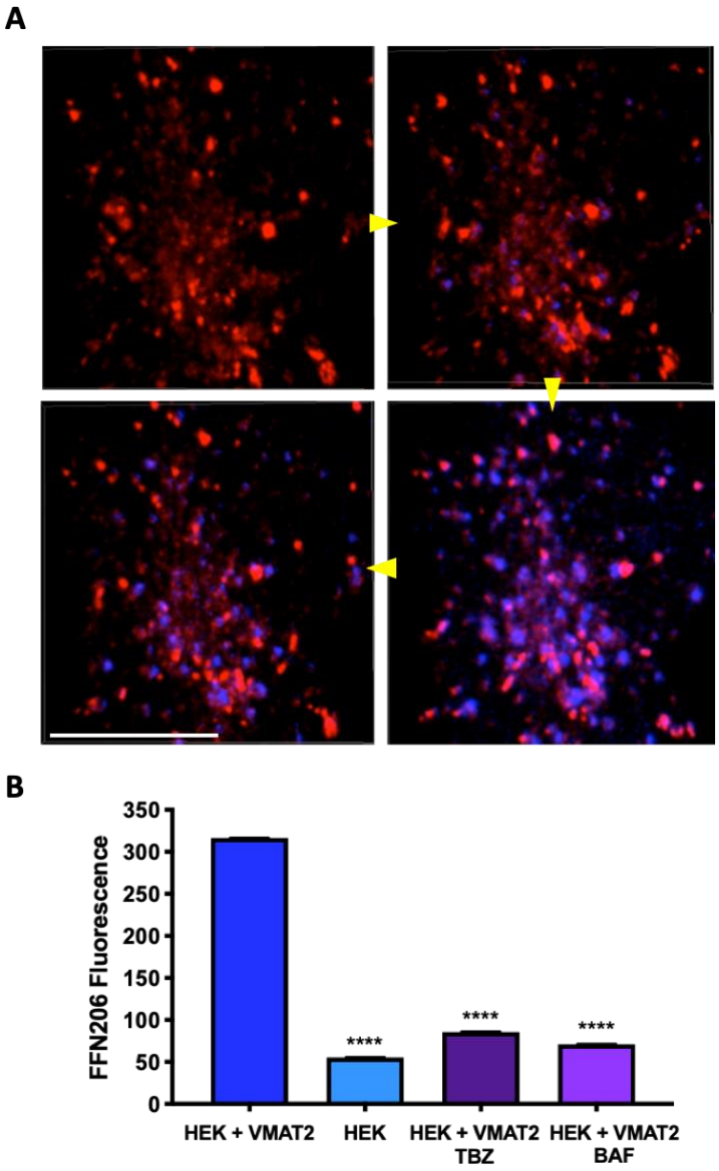

Figure 2. Real-time uptake of FFN206 in a single cell.

A. Sequential stills taken from a video of FFN206 uptake (blue fluorescence) into the vesicle-like compartments of a single HEK cell stably transfected with mCherry-tagged VMAT2 (red fluorescence). Still photos taken at 0.93s, 3.18s, 3.94s, and 5.94s following FFN206 application. Scale bar = 10 µM. Yellow arrows indicate image progression. B. Comparison of peak FFN206 fluorescence in the final 20 seconds of 1000 total seconds of uptake. HEK+VMAT2 cells display significantly greater fluorescence than HEK cells and HEK+VMAT2 cells treated with

402 tetrabenazine or bafilomycin. Bars are displayed as mean and standard error of the mean. (One-
403 way ANOVA with Dunnett's multiple comparisons post-hoc test **** $p < 0.0001$ vs. control
404 column HEK+VMAT2).

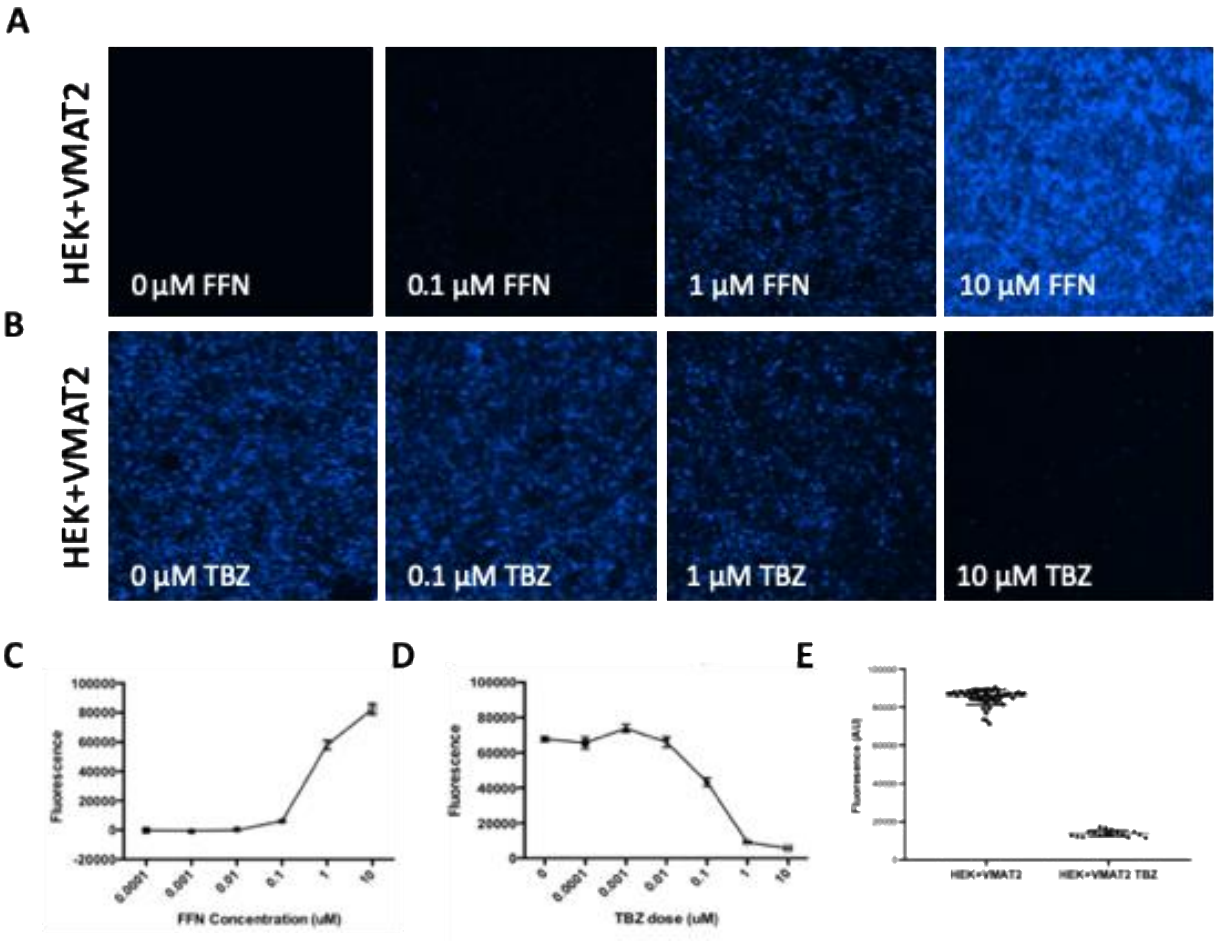

Figure 3. Determining optimal parameters for a FFN206 96-well plate assay.

A. Representative images of HEK+VMAT2 cells treated with 0, 0.1, 1, or 10 µM of FFN206. Cells imaged at 10x magnification. B. Representative images of HEK+VMAT2 cells treated with 0, 0.1, 1, and 10 µM of tetrabenazine (TBZ) and 1 µM FFN206. Cells imaged by EVOS system at 10x magnification. Scale bar = 400 µM. C. Quantification of fluorescence in 3A demonstrating FFN206 fluorescence increases as FFN206 dose increases. D. Quantification of fluorescence in 3B demonstrating FFN206 fluorescence decreases as tetrabenazine dose increases. E. Quantification of FFN206 fluorescence in HEK+VMAT2 cells treated with 1 µM FFN206 and 0 µM TBZ compared to cells treated with 1 µM FFN206 and 10 µM TBZ.

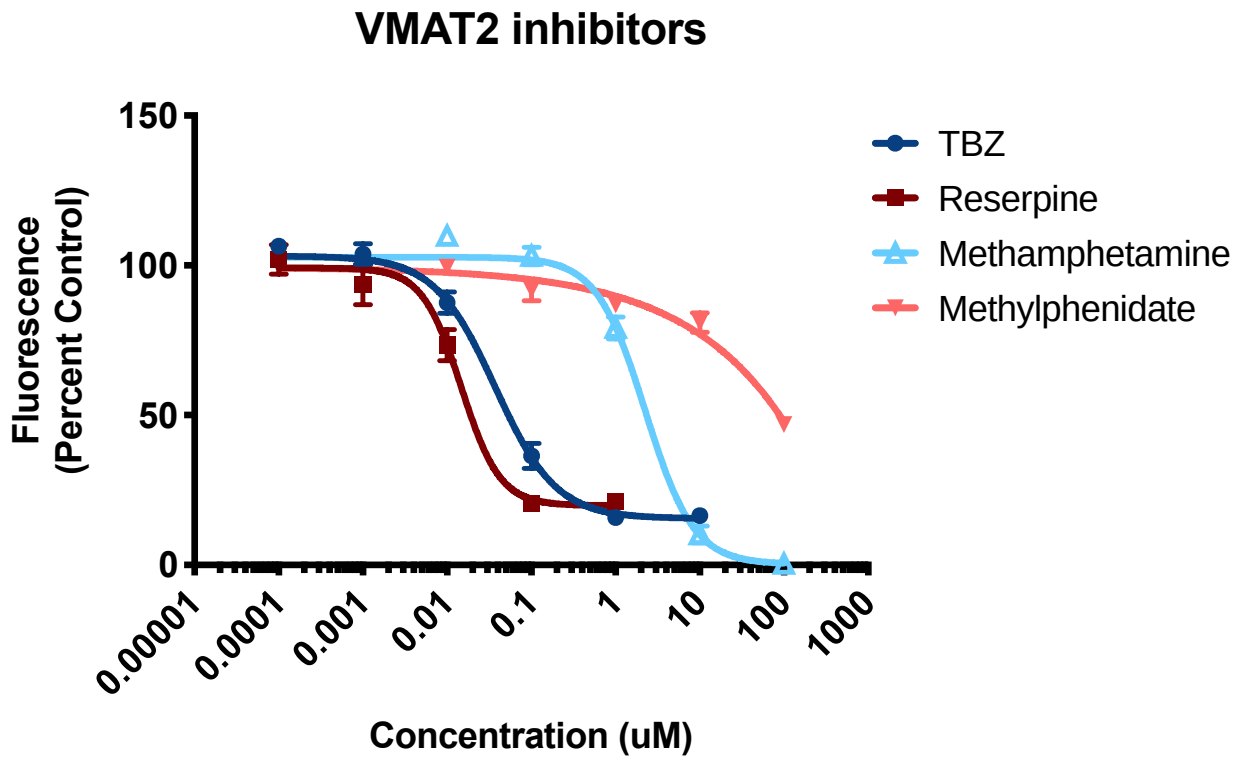

Figure 4. Screening pharmacological inhibitors of VMAT2.

HEK+VMAT2 cells were treated with 0.0001, 0.001, 0.01, 0.1, 1, and 10 µM of tetrabenazine (TBZ); 0.0001, 0.001, 0.01, 0.1, 1, and 10 µM of reserpine; 0.01, 0.1, 1, 10, and 100 µM of methamphetamine; or 0.01, 0.1, 1, 10, and 100 µM of methylphenidate. FFN206 fluorescence represented as percent of control (HEK+VMAT2 cells treated with 0 µM drug). Graphs depict mean and standard error of the mean and curves represent non-linear regressions.

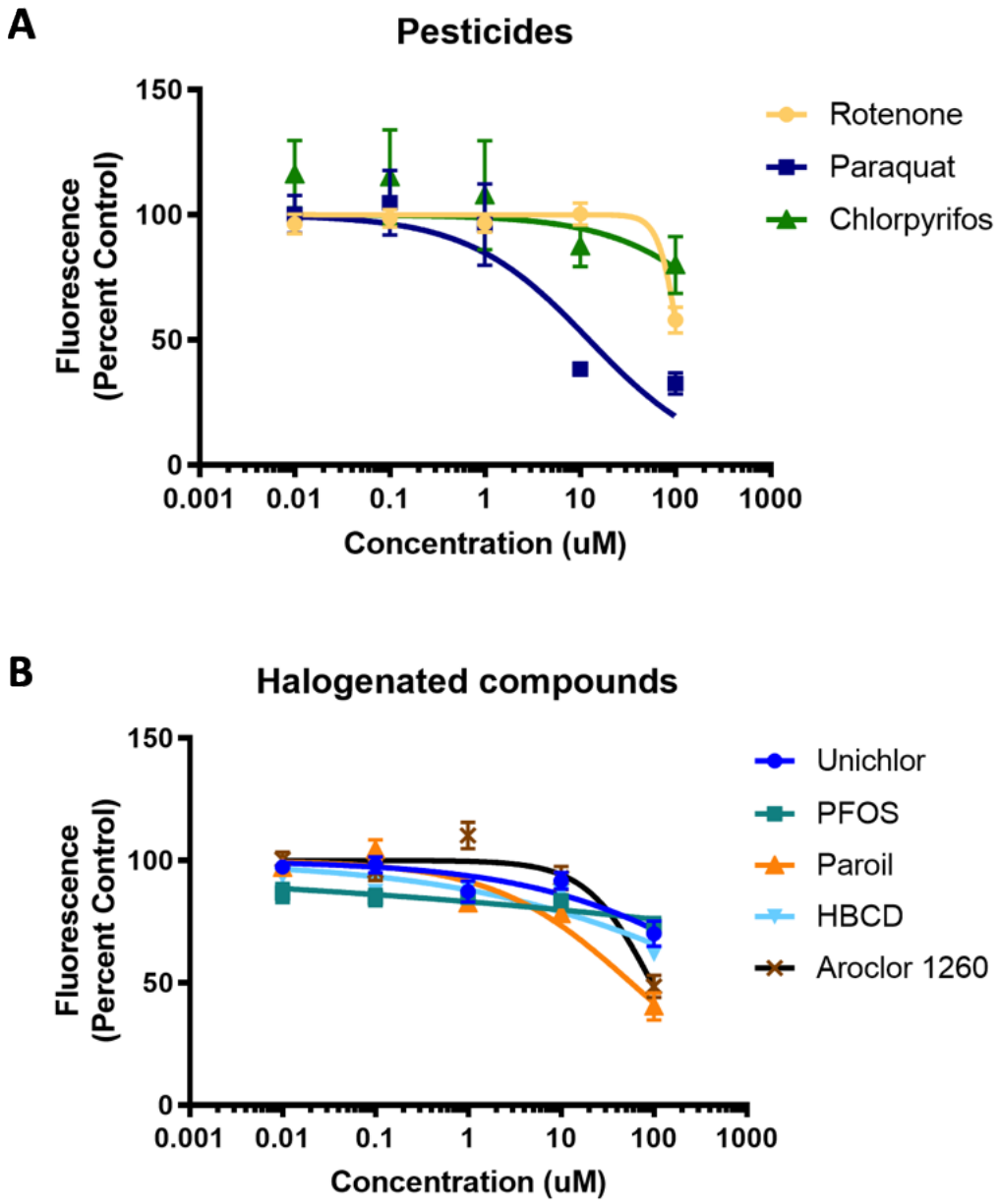

422

423 **Figure 5. Screening environmental toxicants for influence on VMAT2 function.**

424 A. HEK+VMAT2 cells were treated with 0.01, 0.1, 1, 10 and 100 µM of the pesticides rotenone,
425 paraquat, or chlorpyrifos. B. HEK+VMAT2 cells were treated with 0.01, 0.1, 1, 10 and 100 µM
426 of the halogenated compounds unichlor, PFOS, Paroil, hexabromocyclododecane, or Aroclor
427 1260. FFN206 fluorescence represented as percent of control (HEK+VMAT2 cells treated with 0

μM drug). Graphs depict mean and standard error of the mean and curves represent non-linear regressions.

References

1 Alter, S. P., Lenzi, G. M., Bernstein, A. I. & Miller, G. W. Vesicular integrity in Parkinson's disease. *Curr Neurol Neurosci Rep* **13**, 362, doi:10.1007/s11910-013-0362-3 (2013).

2 Chen, L. *et al.* Unregulated cytosolic dopamine causes neurodegeneration associated with oxidative stress in mice. *J Neurosci* **28**, 425-433, doi:10.1523/JNEUROSCI.3602-07.2008 (2008).

3 Graham, D. G., Tiffany, S. M., Bell, W. R., Jr. & Gutknecht, W. F. Autoxidation versus covalent binding of quinones as the mechanism of toxicity of dopamine, 6-hydroxydopamine, and related compounds toward C1300 neuroblastoma cells in vitro. *Mol. Pharmacol.* **14**, 644-653 (1978).

4 Lohr, K. M. *et al.* Vesicular monoamine transporter 2 (VMAT2) level regulates MPTP vulnerability and clearance of excess dopamine in mouse striatal terminals. *Toxicol Sci*, doi:10.1093/toxsci/kfw106 (2016).

5 Lohr, K. M. *et al.* Increased Vesicular Monoamine Transporter 2 (VMAT2; Slc18a2) Protects against Methamphetamine Toxicity. *ACS Chem Neurosci*, doi:10.1021/acschemneuro.5b00010 (2015).

6 Lohr, K. M. *et al.* Increased vesicular monoamine transporter enhances dopamine release and opposes Parkinson disease-related neurodegeneration in vivo. *Proceedings of the National Academy of Sciences of the United States of America* **111**, 9977-9982, doi:10.1073/pnas.1402134111 (2014).

449 7 Bradner, J. M. *et al.* Exposure to the polybrominated diphenyl ether mixture DE-71
450 damages the nigrostriatal dopamine system: role of dopamine handling in neurotoxicity. *Exp*
451 *Neurol* **241**, 138-147, doi:10.1016/j.expneurol.2012.12.013 (2013).

452 8 Guillot, T. S. *et al.* Reduced vesicular storage of dopamine exacerbates methamphetamine-
453 induced neurodegeneration and astrogliosis. *J Neurochem* **106**, 2205-2217, doi:10.1111/j.1471-
454 4159.2008.05568.x (2008).

455 9 Caudle, W. M. *et al.* Reduced vesicular storage of dopamine causes progressive
456 nigrostriatal neurodegeneration. *J Neurosci* **27**, 8138-8148, doi:10.1523/JNEUROSCI.0319-
457 07.2007 (2007).

458 10 Guillot, T. S. & Miller, G. W. Protective actions of the vesicular monoamine transporter 2
459 (VMAT2) in monoaminergic neurons. *Mol Neurobiol* **39**, 149-170, doi:10.1007/s12035-009-
460 8059-y (2009).

461 11 Fumagalli, F. *et al.* Increased methamphetamine neurotoxicity in heterozygous vesicular
462 monoamine transporter 2 knock-out mice. *J Neurosci* **19**, 2424-2431 (1999).

463 12 Gainetdinov, R. R. *et al.* Increased MPTP neurotoxicity in vesicular monoamine
464 transporter 2 heterozygote knockout mice. *J Neurochem* **70**, 1973-1978 (1998).

465 13 Wang, Y. M. *et al.* Knockout of the vesicular monoamine transporter 2 gene results in
466 neonatal death and supersensitivity to cocaine and amphetamine. *Neuron* **19**, 1285-1296 (1997).

467 14 Burke, W. J. *et al.* Neurotoxicity of MAO metabolites of catecholamine neurotransmitters:
468 role in neurodegenerative diseases. *Neurotoxicology* **25**, 101-115, doi:10.1016/s0161-
469 813x(03)00090-1 (2004).

15 Lawal, H. O. *et al.* The Drosophila vesicular monoamine transporter reduces pesticide-induced loss of dopaminergic neurons. *Neurobiol Dis* **40**, 102-112, doi:10.1016/j.nbd.2010.05.008 (2010).

16 Lawal, H. O. *et al.* Drosophila modifier screens to identify novel neuropsychiatric drugs including aminergic agents for the possible treatment of Parkinson's disease and depression. *Mol Psychiatry* **19**, 235-242, doi:10.1038/mp.2012.170 (2014).

17 Langston, J. W., Ballard, P., Tetrud, J. W. & Irwin, I. Chronic Parkinsonism in humans due to a product of meperidine-analog synthesis. *Science* **219**, 979-980 (1983).

18 Liu, Y. & Edwards, R. H. The role of vesicular transport proteins in synaptic transmission and neural degeneration. *Annu Rev Neurosci* **20**, 125-156, doi:10.1146/annurev.neuro.20.1.125 (1997).

19 Staal, R. G. & Sonsalla, P. K. Inhibition of brain vesicular monoamine transporter (VMAT2) enhances 1-methyl-4-phenylpyridinium neurotoxicity in vivo in rat striata. *J. Pharmacol. Exp. Ther.* **293**, 336-342 (2000).

20 Takahashi, N. *et al.* VMAT2 knockout mice: heterozygotes display reduced amphetamine-conditioned reward, enhanced amphetamine locomotion, and enhanced MPTP toxicity. *Proc Natl Acad Sci U S A* **94**, 9938-9943 (1997).

21 Chen, C. X., Huang, S. Y., Zhang, L. & Liu, Y. J. Synaptophysin enhances the neuroprotection of VMAT2 in MPP+-induced toxicity in MN9D cells. *Neurobiol. Dis.* **19**, 419-426, doi:10.1016/j.nbd.2005.01.014 (2005).

22 Liu, Y. *et al.* A cDNA that suppresses MPP+ toxicity encodes a vesicular amine transporter. *Cell* **70**, 539-551 (1992).

23 Mooslehner, K. A. *et al.* Mice with very low expression of the vesicular monoamine transporter 2 gene survive into adulthood: potential mouse model for parkinsonism. *Mol Cell Biol* **21**, 5321-5331, doi:10.1128/MCB.21.16.5321-5331.2001 (2001).

24 Fon, E. A. *et al.* Vesicular transport regulates monoamine storage and release but is not essential for amphetamine action. *Neuron* **19**, 1271-1283 (1997).

25 Alter, S. P. *et al.* Reduced vesicular monoamine transport disrupts serotonin signaling but does not cause serotonergic degeneration. *Exp Neurol* **275 Pt 1**, 17-24, doi:10.1016/j.expneurol.2015.09.016 (2016).

26 Taylor, T. N. *et al.* Nonmotor symptoms of Parkinson's disease revealed in an animal model with reduced monoamine storage capacity. *J Neurosci* **29**, 8103-8113, doi:10.1523/JNEUROSCI.1495-09.2009 (2009).

27 Taylor, T. N., Caudle, W. M. & Miller, G. W. VMAT2-Deficient Mice Display Nigral and Extranigral Pathology and Motor and Nonmotor Symptoms of Parkinson's Disease. *Parkinsons Dis.* **2011**, 124165, doi:10.4061/2011/124165 (2011).

28 Pifl, C. *et al.* Is Parkinson's disease a vesicular dopamine storage disorder? Evidence from a study in isolated synaptic vesicles of human and nonhuman primate striatum. *J Neurosci* **34**, 8210-8218, doi:10.1523/JNEUROSCI.5456-13.2014 (2014).

29 Miller, G. W. *et al.* Immunochemical Analysis of Vesicular Monoamine Transporter (VMAT2) Protein in Parkinson's Disease. *Experimental Neurology* **156**, 138-148 (1999).

30 Rilstone, J. J., Alkhater, R. A. & Minassian, B. A. Brain dopamine-serotonin vesicular transport disease and its treatment. *N Engl J Med* **368**, 543-550, doi:10.1056/NEJMoa1207281 (2013).

31 Glatt, C. E., Wahner, A. D., White, D. J., Ruiz-Linares, A. & Ritz, B. Gain-of-function haplotypes in the vesicular monoamine transporter promoter are protective for Parkinson disease in women. *Human molecular genetics* **15**, 299-305, doi:10.1093/hmg/ddi445 (2006).

32 Brighina, L. *et al.* Analysis of vesicular monoamine transporter 2 polymorphisms in Parkinson's disease. *Neurobiol. Aging* **34**, 1712.e1719-1713, doi:10.1016/j.neurobiolaging.2012.12.020 (2013).

33 Xiong, N. *et al.* hVMAT2: A Target of Individualized Medication for Parkinson's Disease. *Neurotherapeutics* **13**, 623-634, doi:10.1007/s13311-016-0435-5 (2016).

34 Sala, G. *et al.* Vesicular monoamine transporter 2 mRNA levels are reduced in platelets from patients with Parkinson's disease. *J Neural Transm (Vienna)* **117**, 1093-1098, doi:10.1007/s00702-010-0446-z (2010).

35 Caudle, W. M. *et al.* Polychlorinated biphenyl-induced reduction of dopamine transporter expression as a precursor to Parkinson's disease-associated dopamine toxicity. *Toxicol Sci* **92**, 490-499, doi:10.1093/toxsci/kfl018 (2006).

36 Richardson, J. R. *et al.* Developmental exposure to the pesticide dieldrin alters the dopamine system and increases neurotoxicity in an animal model of Parkinson's disease. *FASEB J* **20**, 1695-1697, doi:10.1096/fj.06-5864fje (2006).

37 Ascherio, A. *et al.* Pesticide exposure and risk for Parkinson's disease. *Ann Neurol* **60**, 197-203, doi:10.1002/ana.20904 (2006).

38 Elbaz, A. *et al.* Professional exposure to pesticides and Parkinson disease. *Ann Neurol* **66**, 494-504, doi:10.1002/ana.21717 (2009).

39 Semchuk, K. M., Love, E. J. & Lee, R. G. Parkinson's disease and exposure to agricultural work and pesticide chemicals. *Neurology* **42**, 1328-1335 (1992).

40 Miller, G. W., Kirby, M. L., Levey, A. I. & Bloomquist, J. R. Heptachlor alters expression and function of dopamine transporters. *Neurotoxicology* **20**, 631-637 (1999).

41 Bemis, J. C. & Seegal, R. F. PCB-induced inhibition of the vesicular monoamine transporter predicts reductions in synaptosomal dopamine content. *Toxicol Sci* **80**, 288-295, doi:10.1093/toxsci/kfh153 (2004).

42 Hu, G. *et al.* New fluorescent substrate enables quantitative and high-throughput examination of vesicular monoamine transporter 2 (VMAT2). *ACS Chem Biol* **8**, 1947-1954, doi:10.1021/cb400259n (2013).

43 Zhang, J. H., Chung, T. D. & Oldenburg, K. R. A Simple Statistical Parameter for Use in Evaluation and Validation of High Throughput Screening Assays. *Journal of biomolecular screening* **4**, 67-73 (1999).

44 Bernstein, A. I., Stout, K. A. & Miller, G. W. A fluorescent-based assay for live cell, spatially resolved assessment of vesicular monoamine transporter 2-mediated neurotransmitter transport. *J Neurosci Methods* **209**, 357-366, doi:10.1016/j.jneumeth.2012.06.002 (2012).

551 45 Zhang, H. *et al.* Dopamine release at individual presynaptic terminals visualized with
552 FFNs. *Journal of visualized experiments : JoVE*, doi:10.3791/1562 (2009).

553 46 Gubernator, N. G. *et al.* Fluorescent false neurotransmitters visualize dopamine release
554 from individual presynaptic terminals. *Science* **324**, 1441-1444, doi:10.1126/science.1172278
555 (2009).

556 47 Rodriguez, P. C. *et al.* Fluorescent dopamine tracer resolves individual dopaminergic
557 synapses and their activity in the brain. *Proceedings of the National Academy of Sciences of the*
558 *United States of America* **110**, 870-875, doi:10.1073/pnas.1213569110 (2013).

559 48 Pereira, D. B. *et al.* Fluorescent false neurotransmitter reveals functionally silent dopamine
560 vesicle clusters in the striatum. *Nat Neurosci* **19**, 578-586, doi:10.1038/nn.4252 (2016).

561 49 Lau, T., Proissl, V., Ziegler, J. & Schloss, P. Visualization of neurotransmitter uptake and
562 release in serotonergic neurons. *J Neurosci Methods* **241**, 10-17,
563 doi:10.1016/j.jneumeth.2014.12.009 (2015).

564 50 Freire, C. & Koifman, S. Pesticide exposure and Parkinson's disease: epidemiological
565 evidence of association. *Neurotoxicology* **33**, 947-971, doi:10.1016/j.neuro.2012.05.011 (2012).

566 51 Goldman, S. M. Environmental toxins and Parkinson's disease. *Annu Rev Pharmacol*
567 *Toxicol* **54**, 141-164, doi:10.1146/annurev-pharmtox-011613-135937 (2014).

568 52 Nistico, R., Mehdawy, B., Piccirilli, S. & Mercuri, N. Paraquat- and rotenone-induced
569 models of Parkinson's disease. *Int. J. Immunopathol. Pharmacol.* **24**, 313-322,
570 doi:10.1177/039463201102400205 (2011).

53 Tanner, C. M. *et al.* Rotenone, paraquat, and Parkinson's disease. *Environ Health Perspect* **119**, 866-872, doi:10.1289/ehp.1002839 (2011).

54 Cannon, J. R. & Greenamyre, J. T. Gene-environment interactions in Parkinson's disease: specific evidence in humans and mammalian models. *Neurobiol Dis* **57**, 38-46, doi:10.1016/j.nbd.2012.06.025 (2013).

55 Bove, J. & Perier, C. Neurotoxin-based models of Parkinson's disease. *Neuroscience* **211**, 51-76, doi:10.1016/j.neuroscience.2011.10.057 (2012).

56 Sherer, T. B. *et al.* Mechanism of toxicity of pesticides acting at complex I: relevance to environmental etiologies of Parkinson's disease. *J Neurochem* **100**, 1469-1479, doi:10.1111/j.1471-4159.2006.04333.x (2007).

57 Ramachandiran, S., Hansen, J. M., Jones, D. P., Richardson, J. R. & Miller, G. W. Divergent mechanisms of paraquat, MPP+, and rotenone toxicity: oxidation of thioredoxin and caspase-3 activation. *Toxicol Sci* **95**, 163-171, doi:10.1093/toxsci/kfl125 (2007).

58 Wu, M. *et al.* Regulator of G protein signaling-1 modulates paraquat-induced oxidative stress and longevity via the insulin like signaling pathway in Caenorhabditis elegans. *Toxicol Lett* **273**, 97-105, doi:10.1016/j.toxlet.2017.03.027 (2017).

59 Salgado, R., Lopez-Doval, S., Pereiro, N. & Lafuente, A. Perfluorooctane sulfonate (PFOS) exposure could modify the dopaminergic system in several limbic brain regions. *Toxicol Lett* **240**, 226-235, doi:10.1016/j.toxlet.2015.10.023 (2016).

60 Genskow, K. R., Bradner, J. M., Hossain, M. M., Richardson, J. R. & Michael Caudle, W. Selective damage to dopaminergic transporters following exposure to the brominated flame retardant, HBCDD. *Neurotoxicol Teratol*, doi:10.1016/j.ntt.2015.06.003 (2015).